Interaction of modified oligonucleotides with nuclear proteins, formation of novel nuclear structures and sequence-independent effects on RNA processing

Loren L Flynn #, Ruohan Li # May T Aung-Htut, Ianthe L Pitout, Jack A L Cooper, Alysia Hubbard, Lisa Griffiths, Charlie Bond, Steve D Wilton, Archa H Fox* and Sue Fletcher*

 # authors contributed equally

***corresponding authors**

Abstract (max 150 words)

Oligonucleotides and nucleic acid analogues that alter gene expression are showing therapeutic promise for selected human diseases. The modification of synthetic nucleic acids to protect against nuclease degradation and to influence drug function is common practice, however, such modifications may also confer unexpected physicochemical and biological properties. Here we report backbone-specific effects of modified oligonucleotides on subnuclear organelles, altered distribution of nuclear proteins, the appearance of novel structured nuclear inclusions, and modification of RNA processing in cultured cells transfected with antisense oligonucleotides on a phosphorothioate backbone. Phosphodiester and phosphorodiamidate morpholino oligomers elicited no such consequences. Disruption of subnuclear structures and proteins elicit severe phenotypic disturbances, revealed by transcriptomic analysis of fibroblasts exhibiting such disruption. These data suggest that the toxic effects and adverse events reported after clinical evaluation of phosphorothioate nucleic acid drugs may be mediated, at least in part, by non-specific interaction of nuclear components with the phosphorothioate backbone.

Key Words

Antisense oligonucleotides, RNA analogue, RNA processing, paraspeckle proteins, nuclear organelles

Abbreviations

antisense oligonucleotide (AO), spinal muscular atrophy (SMA), Duchenne muscular dystrophy (DMD) phosphorodiamidate morpholino oligomer (PMO) amyotrophic lateral sclerosis (ALS)

Introduction

Antisense oligonucleotide drugs are a class of therapeutics designed to alter gene expression and function, and are reported to have delivered therapeutic benefit to spinal muscular atrophy (SMA) type 1 patients (Paton 2017) and a subset of Duchenne muscular dystrophy (DMD) cases (Mendell *et al.* 2013, Mendell *et al.* 2016). *Nusinersen* (*Spinraza*) is a 2′O-methoxyethyl antisense oligonucleotide (AO) on a phosphorothioate backbone, targeting a splice silencer (*ISS-N1*) in *SMN2* intron 7 that promotes exon 7 selection during pre-mRNA splicing (Singh *et al.* 2006) and received Food and Drug Administration (USA) (FDA) approval in December 2016 for the treatment of SMA. *Exondys51* is a phosphorodiamidate morpholino oligomer (PMO) that targets the *DMD* pre-mRNA to exclude exon 51, in order to re-frame the dystrophin transcript around frame shifting deletions flanking exon 51, as a treatment for DMD (Mendell *et al.* 2013). *Exondys51* received accelerated approval from the FDA on September 19th 2016. Other drugs exploiting the antisense concept include Kynamro® (mipomersen sodium) (Wong and Goldberg 2014), an adjunctive treatment to reduce LDL-C levels in familial hypercholesteremia, approved in January 2013, followed by an FDA hepatotoxity black box warning; and a number of compounds at various stages of clinical development, predominantly siRNA and oligodeoxyribonucleotide analogues designed to induce RNAse H degradation of target transcripts (for review see (Bennett *et al*. 2017, Stein and Castanotto 2017)). Recently, Alnylam announced the first FDA approval of an RNAi Therapeutic, ONPATTRO™ (patisiran) for the treatment of adult patients with polyneuropathy of hereditary transthyretin-mediated amyloidosis. (https://www.fda.gov/NewsEvents/Newsroom/PressAnnouncements/ucm616518.htm)

Strategies to improve biological stability and confer pharmaceutical properties to nucleic acid drugs include chemical modifications of the bases and nucleic acid backbone to increase resistance to endogenous nucleases; modifications that influence specific oligomer activity and conjugates that enhance cellular uptake and improve tissue distribution. While the phosphorothioate backbone is the most widely applied chemical modification, changes to the ribose moiety (eg, 2′ O-methylation, 2′ O-methoxyethyl, 2′ O-fluoro), nucleobases and other backbone modifications, including peptide nucleic acids and phosphorodiamidate morpholino oligomers can confer specific characteristics and mechanisms of action (for review see (Veedu 2015, Wilton *et al.* 2015, Tri Le *et al.* 2016)).

Many laboratories, including our own, routinely use 2′ O-methyl phosphorothioate oligonucleotides to evaluate antisense sequences for targeted splicing modulation, and different modified bases on a phosphorothioate backbone for various other molecular interventions (Lipi *et al.* 2016, Chakravarthy *et al.* 2017). These compounds can be economically prepared in-house and efficiently transfected into a range of cells as cationic liposomes or dendrimer complexes, using commercially available reagents. However, for sustained splice modification, *in vivo* use and clinical application, PMOs have proved safe and effective (Gebski *et al.* 2003, Fletcher *et al.* 2006, Kinali *et al.* 2009, Mendell *et al.* 2016). We previously reported that antisense exon skipping sequences prepared and optimized *in vitro* as 2′ O-methyl phosphorothioate oligonucleotides generally perform comparably when synthesized as PMO (Adams *et al.* 2007). An extended antisense sequence targeting the *ISS-N1* region of *SMN2* was validated *in vitro* and *in vivo* using 2′ O-methyl phosphorothioate and PMO chemistries (Mitrpant *et al.* 2013).

Phosphorothioate backbone modification of nucleic acid drugs is common practice for protection from rapid degradation by circulating and intracellular nucleases, but these modified AOs can interact undesirably with endogenous cellular components. Early work indicated that negatively charged phosphorothioate AOs bind non-specifically to heparin-like proteins, laminin and collagen (Dias and Stein 2002) and more recently, phosphorothioate AOs were reported to interact with nuclear paraspeckle-associated proteins, sequestering them away from their endogenous target, the long non-coding RNA *NEAT1,* and also seeding paraspeckle like-structures in the absence of *NEAT1* (Shen *et al.* 2014, Shen *et al.* 2015). Paraspeckles and paraspeckle proteins are involved in transcriptional regulation, transport and splicing pathways (Bond and Fox 2009, Naganuma *et al.* 2012). Beyond the paraspeckle-associated subset (Shen *et al.* 2014), phosphorothioate AOs were also reported to bind an additional approximately 50 intracellular proteins (Liang *et al.* 2015) however, these interactions were studied in the context of evaluating the modest impact these interactions had on AO function (Liang *et al.* 2015). A broader question relates to the global consequences on cellular processes arising as a result of the interaction of AOs with nuclear proteins.

Results of *in vivo* studies investigating the consequences of non-specific phosphorothioate AO binding are particularly relevant when considering therapeutic applications. The

sequestration of paraspeckle proteins, in particular proteins of the drosophila behaviour/human splicing (DBHS) family, was associated with acute hepatotoxicity, inflammation and apoptosis after application of 2´ fluoro-modified phosphorothioate antisense oligonucleotides with a 5-10-5 gapmer configuration in mice (Shen *et al.* 2018) and while this study focused on the severity of 2´ fluoro-modified phosphorothioate AOs, all 2´ modifications evaluated have been shown to sequester paraspeckle proteins, albeit to varying degrees (Shen *et al.* 2014, Liang *et al.* 2015, Shen *et al.* 2018). The backbone-dependent binding of phosphorothioate-modified olionucleotides to platelets *in vitro* and *in vivo*, mediated by the platelet-specific receptor glycoprotein VI (GPVI) is also of note (Flierl *et al.* 2015), considering the broad range of nucleic acid therapeutics currently under investigation (for review see (Bennett *et al.* 2017). Oligonucleotides on a phosphorothioate-modified backbone elicited strong platelet activation, signaling, reactive oxygen species generation, adhesion, spreading, aggregation and thrombus formation (Flierl *et al.* 2015). Of particular relevance to current clinical usage, 2´ O-methyl phosphorothioate AOs were reported to activate innate immunity when administered directly to the central nervous system (Toonen *et al.* 2018).

Here we report that transfection of cultured cells with 2´ O-methyl phosphorothioate antisense sequences resulted in numerous novel, large nuclear inclusions in the form of highly structured fibril-like aggregates that co-stained for the paraspeckle proteins, NONO, SFPQ, PSPC1 and FUS. Other nuclear proteins showed altered distribution in 2´ O-methyl phosphorothioate transfected cells. Intranuclear inclusions begin to form within four hours of transfection, and become dominant structures throughout the nucleus within 24 hours. The inclusions appear stable once formed and may remain evident on the culture substrate, even after death and disintegration of the cell. Transmission electron microscopy on transfected cells revealed numerous large, regular structures reminiscent of amyloid deposits, with electron dense regions. Furthermore, gene ontology analyses following RNA sequencing demonstrated significant disruptions to chromatin silencing; regulation of autophagy; nucleotide excision repair; membrane and organelle organization; apoptosis; signalling and protein transmembrane transport, following 2´ O-methyl phosphorothioate transfection.

Materials and Methods

135 *Antisense oligonucleotides*
136 Phosphorodiamidate morpholino oligomers (PMOs) were purchased from Gene-Tools LLC
137 (Philomath, OR, USA), and 2′ O-methyl phosphorothioate AOs were synthesised by TriLink
138 BioTechnologies (San Diego CA, USA). The following sequences were evaluated; an AO
139 encompassing the *SMN* intron 7 *ISS-N1* target, but with a longer sequence *SMN7D(-10-29)*
140 (5′AUUCACUUUCAUAAUGCUGG 3′); the Gene-Tools standard control oligomer, only
141 known to be biologically active in reticulocytes carrying a splice mutation in the human beta-
142 globin pre-mRNA, as an unrelated sham control AO sequence
143 (5′CCUCUUACCUCAGUUACAAUUUAUA 3′), and identified as 'control AO' throughout
144 this study; *Smn* (5′CAC CUU CCU UCU UUU UGA UU 3′) designed to induce exon mouse
145 *Smn* exon skipping and a *SMN* sense AO (5′ CCAGCAUUAUGAAAGUGAAU 3′)
146 complementary to *SMN7D(-10-29)*.
147
148 *Transfection*
149 The 2′O-methyl phosphorothioate AOs were transfected into dermal fibroblasts as lipoplexes
150 using 3 µl of Lipofectamine 3000 (Life Technologies, Melbourne, Australia) per 1 ml of
151 OptiMEM, according to the manufacturer's protocol. The transfection mix was applied to
152 cells seeded at 10,000 per cover slip for immunofluorescence and 15,000 cells per well in 24
153 well plates for RNA extraction and incubated (37°C) for 24 hours prior to RNA and protein
154 analysis. SMA patient fibroblasts were used for the experiments shown in Figures 1f and 1g
155 (Coriell Cell Repositories, GM03813) and fibroblasts from our in-house biobank, obtained
156 from a healthy volunteer, with informed consent (Murdoch University Human Research
157 Ethics Committee Approval #2013/156) were used for all other experiments, except live-cell
158 imaging (see below).
159
160 PMOs were delivered to cells either uncomplexed (10 µM), annealed to a complementary
161 sense DNA oligonucleotide (phosphodiester leash) and transfected as a lipoplex (200 nM), or
162 by nucleofection using a Nucleofector™ X Unit (Lonza, Melbourne, Australia) according to
163 the manufacturer's instructions. PMOs were delivered using the P2 nucleofection kit and CA-
164 137 program at 1 µM, as determined by the final transfection volume. All PMO transfections
165 were incubated for 72 hours prior to RNA and protein analysis.
166
167 *RT-PCR on AO transfected cells*
168 RNA was extracted using the MagMAX-96 Total RNA Isolation Kit, including DNase

169 treatment (Life Technologies), according to the manufacturer's instructions. RT-PCRs were
170 performed using the One-step Superscript III RT-PCR kit with Platinum Taq polymerase (Life
171 Technologies) according to the manufacturer's instructions. All primer sequences and PCR
172 conditions used in this study are detailed in Supplementary File 1**, Table 1**.
173
174 *cDNA synthesis and quantitative PCR*
175 cDNA was synthesised from (~500 ng) RNA extracted from treated and untreated cell cultures
176 using the Superscript IV first-strand synthesis system (Life Technologies) as per the
177 manufacturer's instructions. Prior to qPCR amplification, cDNA was diluted in RNase/DNase
178 free water (1:5).
179
180 The qPCR reactions were performed using Fast SYBR™ Green Master Mix (ThermoFisher
181 Scientific, Melbourne, Australia) and primers for ribosomal RNA subunits *5S* (100% primer
182 efficiency), *18S* (95% primer efficiency), *45S* (100% primer efficiency) and housekeeping Tata
183 box protein (*TBP;*100% primer efficiency) and beta Tubulin (*TUBB;*94% primer efficiency)
184 transcripts. All primer sequences and cycling conditions used in this study are detailed in
185 Supplementary File 1, **Table 1.** Transcript abundance was measured using the CFX384 Touch™
186 Real Time PCR detection system (Bio-Rad Laboratories Pty., Ltd., Gladesville, Australia). The
187 relative expression of each ribosomal RNA subunit to *TBP* and *TUBB* mRNA was calculated
188 using the $2^{-\Delta\Delta CT}$ method and presented as a fold change compared to untreated cells.
189
190 *Immunofluorescence*
191
192 Approximately 10,000 fibroblasts were seeded onto 22 mm x 22 mm coverslips in
193 6-well plates and incubated for 24 hours, prior to transfection. Following transfection,
194 the cells were fixed using acetone:methanol (1:1) on ice for 4 minutes and air-dried.
195
196
197 Fixed cells were washed in PBS containing 1% Triton X-100 to permeabilise the
198 nuclear membrane, and then in PBS to remove excess Triton X-100. Primary antibodies
199 were diluted in PBS containing 0.05% Tween20 and applied to cells for 1 hour at room
200 temperature. All antibody details and staining conditions are listed in Supplementary File
201 1 **Table 2**. Primary antibodies were detected using AlexaFluor488 anti-mouse (cat no.
202 A11001), anti-rabbit (cat. No A11008) or AlexaFluor568 anti-mouse (cat. No A11004) or
203 anti-rabbit (cat. No A11011) (1:400) after incubation for 1 hour at room temperature, and

204 counterstained with Hoechst 33342 (Sigma-Aldrich) for nuclei detection (1 mg/ml, diluted
205 1:125).
206
207 *Western blotting*
208 Cell lysates were prepared with 125 mM Tris/HCl pH 6.8, 15% SDS, 10% Glycerol, 1.25 µM
209 PMSF (Sigma-Aldrich, NSW, Australia and 1x protease inhibitor cocktail (Sigma-Aldrich)
210 and sonicated 6 times (1 second pulses) before adding bromophenol blue (0.004%) and
211 dithiothreitol (2.5 mM). Samples were heated at 94°C for 5 minutes, cooled on ice and
212 centrifuged at 14,000 x g for 2 min before loading onto the gel.
213
214 Total protein (10 µg), measured by BCA, was loaded per sample on a NuPAGE Novex 4-12%
215 BIS/Tris gel (Life Technologies) and separated at 200 V for 55 minutes. Proteins were
216 transferred onto a Pall Fluorotrans polyvinylidene fluoride (PVDF) membrane at 350 mA for
217 2 hours. Following blocking for 1 hour, the membrane was incubated in 5% skim milk
218 powder in 1x TBST containing the primary antibody diluted as shown in Supplementary File
219 1, **Table 2.** Immunodetection was performed using the Western Breeze Chemiluminescent
220 Immunodetection System (Life Technologies) according to the manufacturer's instructions.
221 Western blot images were captured on a Vilber Lourmat Fusion FX system using Fusion
222 software and Bio- 1D software was used for image analysis.
223
224
225 *Live cell imaging*
226 U2OS cells, previously modified to tag the endogenous SFPQ gene with GFP were used for
227 live-cell imaging (Li *et al.* 2017). Cells were seeded at 1.5 x 10^5 cells per well in a 12-well
228 plate, 24 hours before transfection, with high glucose DMEM (Life Technologies, Cat
229 No.11995065) supplemented with 10% fetal calf serum and 1% penicillin-streptomycin. On
230 the following day, cells in each well were transfected with 100 nM 2´ O-methyl
231 phosphorothioate AOs complexed with 2.2 µl Lipofectamine 3000 following the
232 manufacturer's instructions. Immediately after transfection, the plate was transferred to an
233 Incucyte S3 (Essen Bioscience) for live-cell imaging at 1 hour intervals under 10 x optical
234 zoom. SFPQ-GFP and activated caspase-3/7 were visualised under standard green and red
235 channels. Incucyte Caspase-3/7 Red Apoptosis Assay Reagent (Essen Bioscience, Cat No.
236 4704) was used to reveal cell apoptosis events.
237

238 *High resolution microscopy*
239 SIM imaging was performed using an N-SIM microscope (Nikon Corporation, Tokyo, Japan),
240 with SR Apochromat TIRF 100 x 1.49 NA oil immersion objective. Spherical aberration was
241 reduced using the Ti2 automated correction collar at the beginning of the imaging session.
242 Images were acquired using 405 nm, 488 nm and 561 nm lasers, with stacks of step size 0.12
243 µm (with top and bottom of samples determined visually), using 3D-SIM mode. Images were
244 reconstructed with NIS Elements software (Nikon Corporation, Tokyo, Japan).
245
246 *Transmission electron microscopy*
247 Following transfection, cells were washed in PBS and fixed in cold 2.5% phosphate buffered
248 glutaraldehyde overnight. The fixed cells were scraped and centrifuged, then embedded in 4%
249 agarose. The pellets were processed using a Leica tissue processor, moving through 1%
250 aqueous osmium tetroxide, increasing graded alcohols, propylene oxide, propylene
251 oxide/araldite mix, and finally pure araldite resin. The osmicated cells, surrounded by resin in
252 a beem capsule were polymerised overnight at 80°C to form hard blocks.
253 Semi-thin (0.5 micron) sections were taken from the blocks using glass knives, on an RMC
254 ultratome, and stained with methylene blue (0.1% aqueous Methylene Blue with 0.1%
255 Borax) to visualise available cells. Ultrathin sections were then cut from selected blocks,
256 using a Diatome diamond knife, at approximately 95 nm thickness and mounted on copper
257 mesh grids and stained with uranyl acetate (5% uranyl acetate solution in 5% aqueous acetic
258 acid) and Reynold's lead citrate. The grids were viewed using a JEOL 1400 TEM, at 80 kV
259 and images captured by an 11-megapixel GATAN digital camera at varying magnifications.
260
261 *RNA sequencing and analysis*
262 RNA quality was confirmed using a Bioanalyser (Perkin Elmar, MA, USA) prior to
263 RNAseq. Samples were sent to the Australian Genome Research Facility (AGRF, Perth and
264 Melbourne, Australia) for whole transcriptome library preparation using the TruSeq Stranded
265 Total RNA Library Prep Kit (Illumina, CA, USA) and ribosomal RNA depletion with the
266 Ribo-Zero-Gold kit (Illumina, CA, USA). Sequencing was performed using an Illumina
267 HiSeq 2500 (Illumina, CA, USA) to generate 100 base pair single end reads, resulting in an
268 average 25 million reads per sample. Raw sequencing files were quality checked using
269 FastQC (0.11.7), with all files passing. No adapter contamination was identified, and reads
270 were not trimmed. Transcript quantification was performed with salmon (0.8.2), using an
271 index constructed from the Ensembl GRCh38.93 annotation. Transcript abundance was

272 summarised to gene-level counts and imported into R using tximport (1.4.0). Differential
273 expression analysis was performed using DESeq2 (1.16.1) and the default parameters (alpha
274 = 0.1). The heatmap of differentially expressed genes ($p_{adj} < 0.1$) was constructed using the
275 heatmap.2 function from R package gplots (3.0.1). Gene ontology analysis was performed
276 using GSEA (3.0) with 1000 gene set permutations. The gene ontology network was
277 constructed using the Enrichment Map plugin for Cytoscape (3.5.1), with cut-offs: $p < 0.05$,
278 FDR < 0.1 and edge > 0.3.
279
280 **Results**
281
282 *Formation of nuclear inclusions after 2´ O-methyl phosphorothioate AO transfection*
283 The phosphorothioate backbone can interact non-specifically with both intra- and extra-
284 cellular proteins, and recruits paraspeckle proteins and forms paraspeckle-like structures
285 when transfected into Hela cells (Shen *et al.* 2014). However, the dynamics of the formation
286 of these structures, as well as the long-term consequences of these structures on cell
287 physiology remain unknown.
288
289 In this study, we largely focused on two 2´ O-methyl phosphorothioate AOs, one that
290 promotes *SMN2* exon 7 retention during splicing by targeting the *ISS-N1* intronic silencer
291 motif (Singh *et al.* 2006) and the other a control oligomer sequence reported by Genetools
292 LLC and widely used as a transfection control, although additional AO sequences were also
293 tested in some experiments, as indicated below. In order to follow nuclear inclusion
294 formation, we first transfected 2´ O-methyl phosphorothioate AO as lipoplexes (100 nM)
295 into U2OS cells expressing genome engineered GFP-labelled endogenous SFPQ (Li *et al.*
296 2017) and performed live cell imaging over 48 hours (**Figure 1a**). The AO transfection
297 induced formation of nuclear inclusions within 5 hours, and over a period of 12 hours, all of
298 the SFPQ within the nucleus is observed sequestered within the inclusions, as revealed by
299 decreased SFPQ staining of the nucleoplasm. Ultimately, only the inclusions are evident, at
300 which time, the inclusions then coalesce into discrete filaments.
301
302 Immunofluorescent staining of the paraspeckle protein, NONO, showed colocalization in
303 nuclear inclusions in fibroblasts transfected with 2´ O-methyl phosphorothioate *SMN7D(-10-*
304 *29)* sequence at 100 nM concentration, but were also evident at AO concentrations as low as
305 12.5 nM within 24 hours of transfection (**Figure 1b**). Of note, the untreated cells show

306 diffuse nucleoplasmic NONO signal, as well as naturally occurring punctate NONO inside
307 endogenous paraspeckle nuclear bodies (Fox *et al.* 2018) (eg. **Figure 1b** (ii)). Nuclear
308 inclusions were also observed following 2′O-methyl phosphorothioate AO transfection into
309 normal human myoblasts, transformed mouse *H2K* myoblasts, and the neuroblastoma SH-
310 SY5Y cell line (Supplementary File 1, **Figure 1).** Once formed, the inclusions appear to be
311 highly stable, and remain evident on the culture substrate following cell death and nuclear
312 fragmentation and blebbing **(Figure 1c (i-ii)).** The nuclear inclusions appear as either long
313 'filaments', punctate foci, or both (**Figure 1c (iii)**). In the past we have routinely observed
314 marked cell death associated with transfection of 2′ O-methyl phosphorothioate AOs into
315 primary cells and cell lines, and hence explored any correlation between cell death and the
316 formation of AO-induced nuclear inclusions. Indeed, we observed here that transfection with
317 2′ O-methyl phosphorothioate AO sequences induced nuclear inclusions that correlated with
318 reduced cell survival (**Figure 1d-e**).
319
320 While transfection of AOs with phosphorothioate and phosphodiester backbones have been
321 demonstrated to result in nuclear inclusions (Shen *et al.* 2014), PMOs are yet to be evaluated
322 in this context. We therefore transfected fibroblasts with the AO sequences described above,
323 synthesized as PMOs. Transfection of the PMO sequences into fibroblasts did not alter the
324 apparent distribution of NONO, nor of any other nuclear proteins studied (**Figure 1f).** In
325 order to demonstrate that poor cellular uptake of these compounds was not a factor, PMOs
326 were transfected using three established delivery techniques known to lead to altered target
327 gene expression; uncomplexed PMO (10 μM), nucleofection (1 μM), and annealed to a
328 complementary DNA "leash" and transfected as a lipoplex (200 nM), all incubated for 72
329 hours after transfection (**Figure 1f (i-iii),** respectively). Immunofluorescent detection of
330 NONO showed no PMO-induced intranuclear inclusion formation or altered distribution of
331 NONO following transfection, under any of the conditions used, and was reproducible,
332 irrespective of the PMO sequence (data not shown). Transfection efficiency and altered exon
333 selection in the target *SMN2* transcript was assessed by RT-PCR across *SMN* exons 4-8,
334 confirming that the absence of intranuclear inclusions in PMO transfected cells was not a
335 consequence of poor uptake of PMO (**Figure 1g**).
336
337
338
339

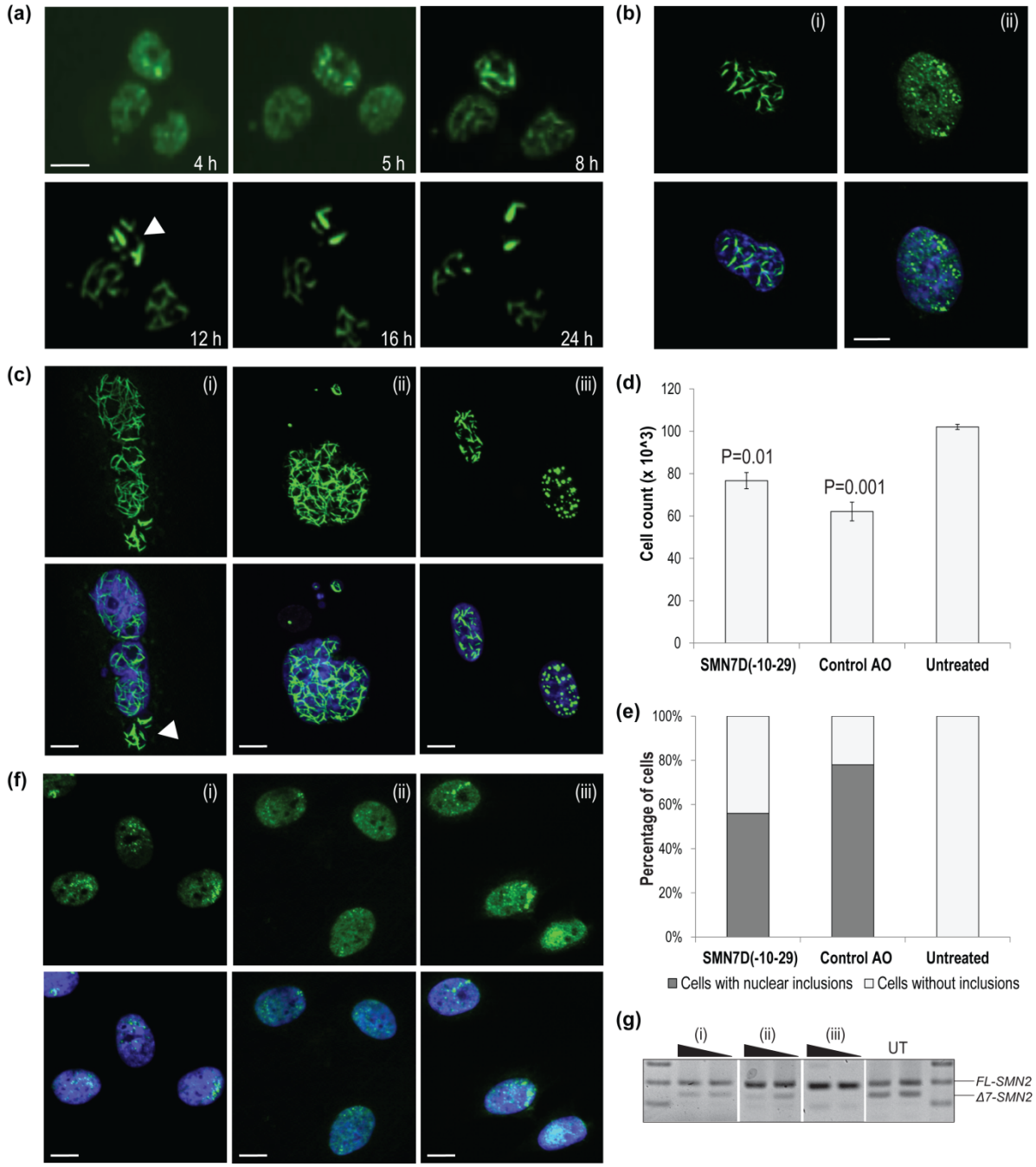

Figure 1 Formation of nuclear inclusions showing **(a)** live cell imaging time-course of U2OS cells with endogenous SFPQ-GFP showing the formation of nuclear inclusions over 24 hours following 2´ O-methyl phosphorothioate control AO transfection (100 nM), inclusions are indicated by the white arrow; **(b)** fibroblasts transfected with 12.5 nM of 2´ O-methyl phosphorothioate *SMN7D(-10-29)* stained for NONO (i), compared to untreated fibroblasts (ii); **(c)** fibroblasts stained for NONO show, (i) nuclear inclusions without evidence of nuclear staining after 2´ O-methyl phosphorothioate *SMN7D(-10-29)* transfection, (ii) nuclear blebbing after 2´ O-methyl phosphorothioate control AO transfection and (iii) nuclear inclusions in the form of filaments or foci induced by transfection with a 2´ O-methyl phosphorothioate *SMN7D(-10-29)* sense sequence AO; **(d)** graph showing the number of viable fibroblasts following 2´ O-methyl phosphorothioate AO transfection (n=4), error bars represent standard error of the mean and P-values calculated using a paired student T-test; **(e)** graph showing the percentage of fibroblasts containing nuclear inclusions following 2´ O-methyl phosphorothioate transfection; **(f)**

353 fibroblasts stained for NONO after transfection with PMO *SMN7D(-10-29)* at (i) high dose un-complexed (10 µM),
354 (ii) using a complementary leash and transfection reagent (200 nM) and (iii) using electroporation (1 µM), all
355 incubated for 72 hours; and **(g)** RT-PCR of full length (FL) and exon 7 skipped (Δ7) *SMN2* transcripts of RNA
356 collected following transfections as in **(f)**. All scale bars = 10 µm.
357

358 To further explore whether AO-induced nuclear inclusions are sequence independent, ninety
359 2′ O-methyl phosphorothioate AOs targeting structural gene transcripts, transcription factors,
360 splicing factors and enzymes, were transfected into fibroblasts and the cells were
361 immunostained for SFPQ (Supplementary File 1, **Table 3)**. All AOs tested disrupted SFPQ
362 distribution and all but one AO formed nuclear inclusions by 24 hours following AO
363 transfection at 100 nM, irrespective of length (18-30 bases) and nucleotide composition
364 (Supplementary File 1, **Table 3**), indicating that with optimal transfection efficiency, any 2′
365 O-methyl phosphorothioate sequence is likely to induce nuclear inclusions. One transfected
366 AO induced NONO localization to the nuclear envelope (Supplementary File 1, **Figure 2a**),
367 while a number of AO sequences induced cytoplasmic SFPQ aggregates in addition to
368 nuclear inclusions (Supplementary File 1, **Figure 2b**). The AO-mediated cytoplasmic
369 aggregate formation was also reported by Liang *et al.,* 2014, who observed cytoplasmic
370 structures as a consequence of TCP1-beta subunit interaction with phosphorothioate-AOs in
371 the cytoplasm, in addition to formation of nuclear 'phosphorothioate bodies', and concluded
372 that upon transfection, the TCP1 proteins interact with phosphorothioate AOs and enhance
373 antisense activity (in this case, activation of the RNase H-mediated target degradation)
374 (Liang *et al.* 2015).
375

376 *Composition of nuclear inclusions induced by 2′ O-methyl phosphorothioate AO transfection*
377 The structure and composition of nuclear inclusions was further investigated by
378 immunostaining of additional selected nuclear proteins found in paraspeckles, the nuclear
379 envelope, nucleoli, nuclear speckles, Cajal bodies and nuclear stress bodies. The paraspeckle
380 proteins PSPC1 and FUS were evident in nuclear inclusions (Supplementary File 1, **Figure**
381 **3a and 3b)** and seen to co-localise with NONO and SFPQ positive inclusions (data not
382 shown), while the proteins TDP-43 and hnRNP-A1 were not observed to be components of
383 nuclear inclusions (Supplementary File 1, **Figure 3c and 3d).**
384

385 Coilin, a component of nuclear Cajal bodies, shows altered distribution in 2′ O-methyl
386 phosphorothioate control AO transfected cells and is distributed evenly through the
387 nucleoplasm and cytoplasm of transfected cells showing NONO-positive nuclear inclusions,

388

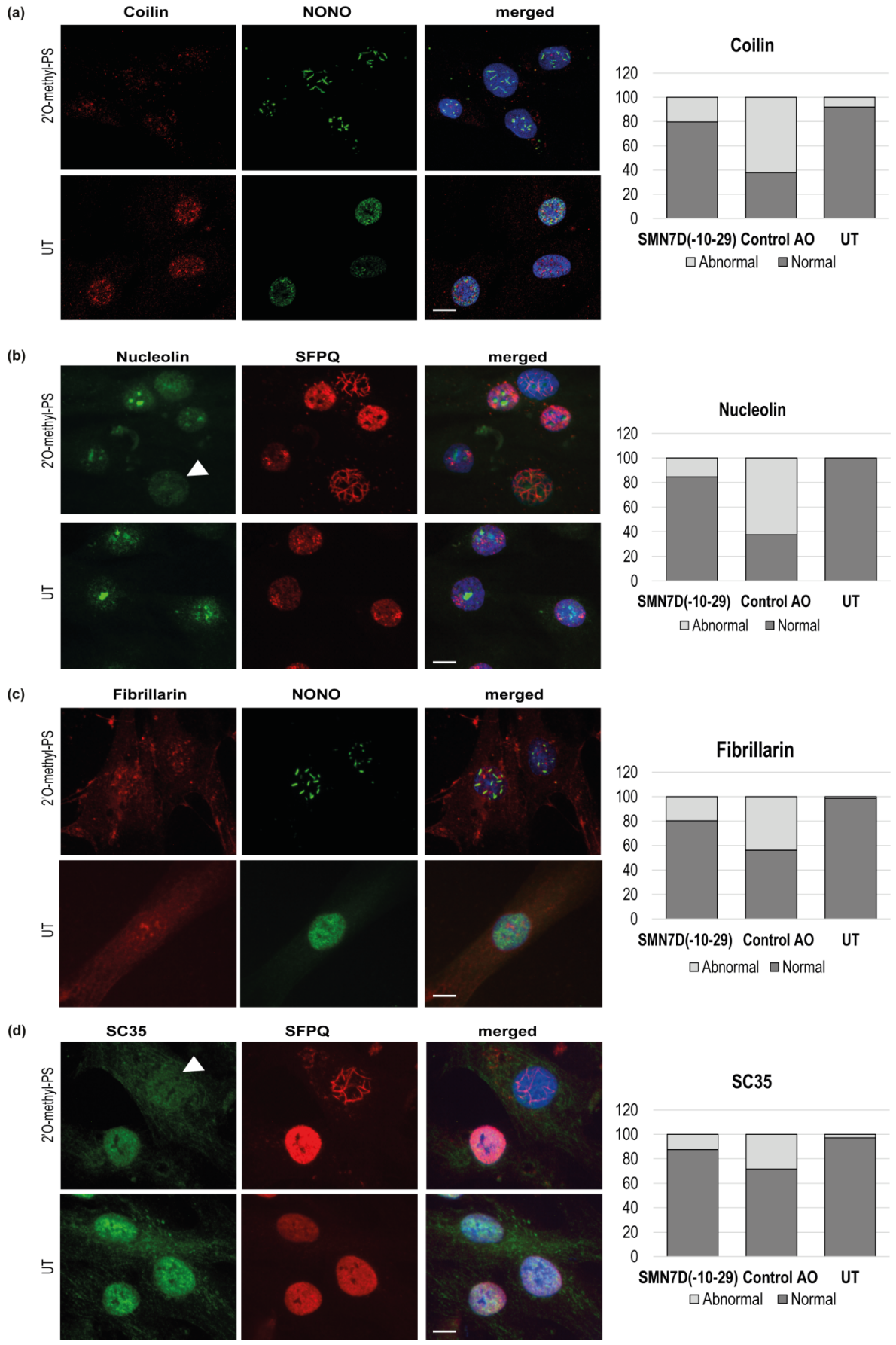
(a)
Coilin
NONO
merged
2'O-methyl-PS
UT
Coilin
120
100
80
60
40
20
0
SMN7D(-10-29)
Control AO
UT
Abnormal
Normal
(b)
Nucleolin
SFPQ
merged
2'O-methyl-PS
UT
Nucleolin
120
100
80
60
40
20
0
SMN7D(-10-29)
Control AO
UT
Abnormal
Normal
(c)
Fibrillarin
NONO
merged
2'O-methyl-PS
UT
Fibrillarin
120
100
80
60
40
20
0
SMN7D(-10-29)
Control AO
UT
Abnormal
Normal
(d)
SC35
SFPQ
merged
2'O-methyl-PS
UT
SC35
120
100
80
60
40
20
0
SMN7D(-10-29)
Control AO
UT
Abnormal
Normal

389

390 **Figure 2** Staining of nuclear bodies following 2´O methyl phosphorothioate transfection (100 nM, 24 hours), with
391 AOs as indicated in cells; **(a)** transfected with the control AO showing coilin (green) and NONO (red) overlayed
392 with hoechst (blue), and graph showing the percentage of abnormal and normally stained cells in cultures
393 transfected with *SMN7D(-10-29)* and control AOs; **(b)** transfected with *SMN7D(-10-29)* showing nucleolin (green)
394 and SFPQ (red) overlayed with hoechst (blue), and graph showing the percentage of abnormal and normally
395 stained cells in cultures transfected with *SMN7D(-10-29)* and control AOs*;* **(c)** transfected with the control AO
396 showing fibrillarin (green) and NONO (red) overlayed with hoechst (blue), and graph showing the percentage of
397 abnormal and normally stained cells in cultures transfected with with *SMN7D(-10-29)* and control AOs and **(d)**
398 transfected with *SMN7D(-10-29)* showing SC35 (green) and SFPQ (red) overlayed with hoechst (blue), and
399 graph showing the percentage of abnormal and normally stained cell in cultures transfected with *SMN7D(-10-29)*
400 and control AOs. All scale bars = 10 µm.
401
402 whereas it is present almost exclusively in the nucleus of untreated cells (**Figure 2a).**
403 Nucleolin and fibrillarin, both markers for the nucleolus, show altered distribution in nuclear
404 inclusion-containing cells, changing from nucleolar to diffuse nucleoplasmic, as shown in
405 **Figures 2b** and **2c**, respectively. The splicing factor and component of nuclear speckles,
406 SC35, showed enhanced cytoplasmic localisation in cells that also contained nuclear
407 inclusions, revealed here by SFPQ immunofluorescence (**Figure 2d**).
408
409 The percentage of AO transfected cells showing disrupted staining or abnormal localization
410 of coilin, nucleolin, fibrillarin and SC35 staining correlated with cells containing
411 intranuclear inclusions, as indicated in the graphs (**Figure 2a-d**). Line intensity profiling
412 shows altered distribution of these nuclear proteins in individual cells that have nuclear
413 inclusions, and is presented in Supplementary File 1, **Figure 4.** Since components of
414 subnuclear organelles were disorganised following transfection with phosphorothioate AOs,
415 the levels of these proteins in the transfected cells were investigated. Western blot analysis
416 showed that the overall abundance of each protein studied to be essentially unchanged
417 following AO transfection. Representative western blots probed for SFPQ, NONO, TDP43,
418 hnRNP-A1, NCL, HSF1 and beta actin, are shown in Supplementary File 1, **Figure 5**.
419
420 *Morphology of 2´ O-methyl phosphorothioate AO-induced nuclear inclusions*
421 Detailed analysis of the 2′ O-methyl phosphorothioate *SMN7D(-10-29)*AO-induced nuclear
422 inclusions was performed using transmission electron microscopy (TEM) on ultra-thin,
423 osmium stained sections (**Figure 3a(i-vi))**. The nuclear inclusions appeared to be
424 microfibrillar or amyloid-like, approximately 200-250 nm in diameter, occurring mostly in
425 groups or bundles. For reference, the width of a DNA double helix is ~2 nm. If captured in a
426 suitable plane of section, the structures appear to have very electron dense termini. Such

427 nuclear inclusions have never before been revealed by transmission electron microscopy in
428 the investigating laboratory. The electron dense regions are reminiscent of perichromatin in
429 size and electron density, the inclusions revealed by TEM extend to ~ 2000 nm in length.
430 Numerous small, partially formed inclusions are also evident in nuclei of transfected cells
431 when viewed at higher magnification (**Figure 3a (iii)**).
432
433 Since transmission electron microscopy can only capture segments of the presumed large
434 fibril-like nuclear inclusions, super resolution microscopy was used to examine 2´ O-methyl
435 phosphorothioate *SMN7D(-10-29)* AO transfected and untreated fibroblasts (**Figure 3b-c**).
436 AO transfected fibroblasts co-stained for NONO and SFPQ show a network of many nuclear
437 inclusions characterised by co-localisation of the two proteins, whereas the untreated cells
438 show more even, punctate distribution within paraspeckles (**Figure 3b (i, ii),** respectively).
439 Transfected fibroblasts co-stained for SFPQ and FUS reveal large interconnected fibril-like
440 structures decorated with FUS at mid-points and at the termini (**Figure 3c (i)**). SFPQ, NONO
441 and FUS are all sequestered to the nuclear inclusions, unlike the even nuclear distribution of
442 these proteins in untreated cells (**Figure 3c (ii)**).
443
444 The nuclear envelope protein, lamin B1 showed altered distribution in a proportion of 2´ O-
445 methyl phosphorothioate *SMN7D(-10-29)* transfected cells that exhibited nuclear inclusions
446 (**Figure 3d (i-ii)**). In these cells, the nuclear envelope labelled by immunostaining of lamin
447 B1 appears multi lobular and distorted, reminiscent of those found in the premature ageing
448 disease progeria and in E145K cells (Taimen *et al.* 2009). A single z-frame image is shown
449 in **Figure 3d (i)** that clearly illustrates lamin B1 localized in 4 distinct nuclear lobules.
450 **Figure 3d (ii and iii)** shows the composite image and an image of an immunostained,
451 untreated fibroblast. In all images (**Figure 3b-d**), the nuclear inclusions appear to reside
452 between areas that may reflect chromosomal territories.

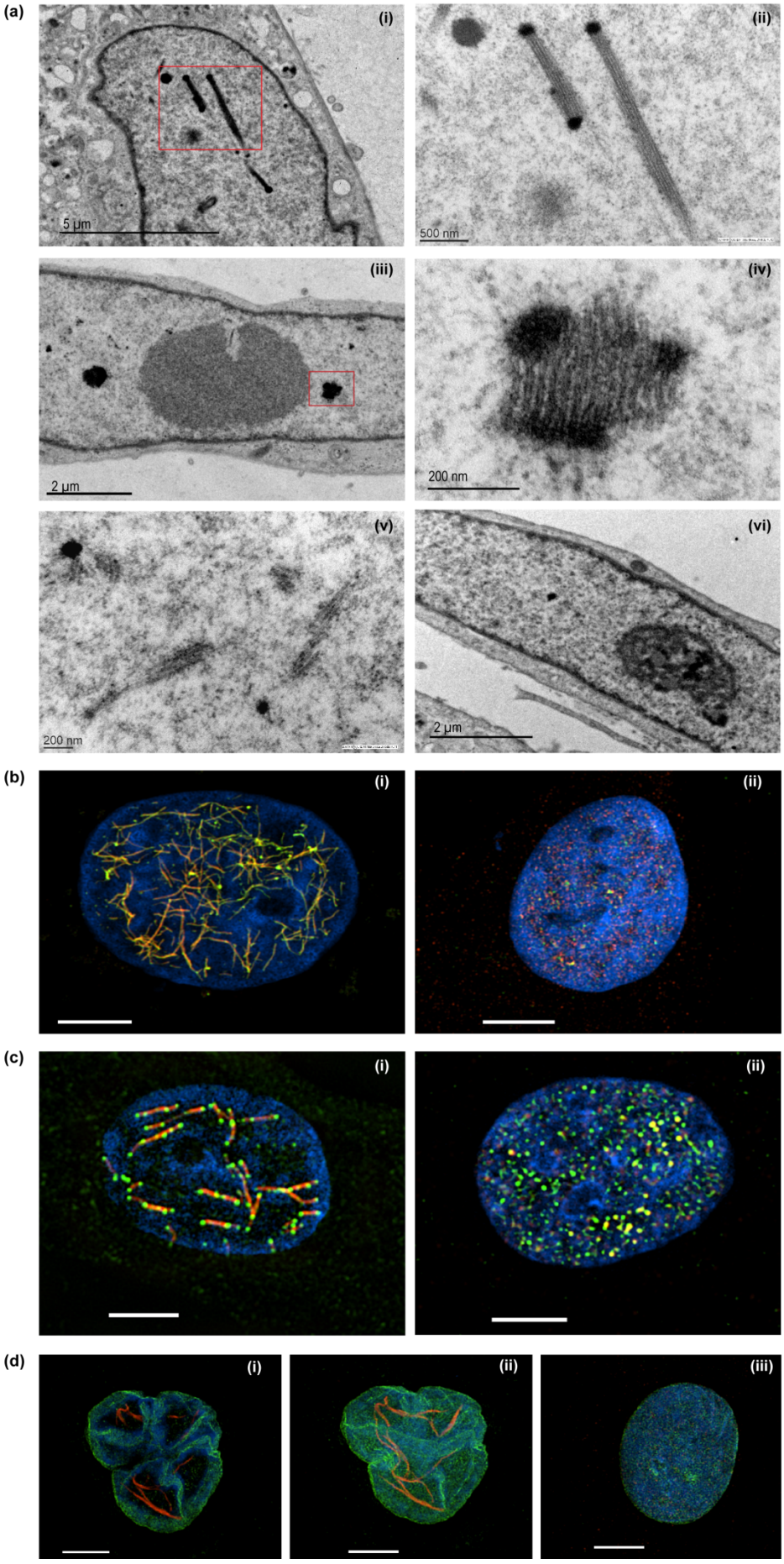
(a)
(i)
5 µm
(ii)
500 nm
(iii)
2 µm
(iv)
200 nm
(v)
200 nm
(vi)
2 µm
(b)
(i)
(ii)
(c)
(i)
(ii)
(d)
(i)
(ii)
(iii)

453

454 **Figure 3** Structural analysis of nuclear inclusions in 2´ O-methyl phosphorothioate *SMN7D(-10-29)* transfected
455 fibroblasts (100 nM, 24 hours), showing **(a)** transmission electron microscopy of (i) nucleus with filament-like
456 nuclear inclusions (scale = 5 µm), (ii) higher magnification of (i) (scale = 500 nm), (iii) nucleus with foci-like
457 nuclear inclusions (scale = 2 µm), (iv) higher magnification of (iv) (scale = 200 nm), (v) partially formed nuclear
458 inclusions (scale = 200 nm), and (vi) untreated nucleus (scale = 2 µm); **(b)** super resolution fluorescence
459 microscopy of SFPQ (green) and NONO (red) co-staining following 2´OMethyl transfection (i) and an untreated
460 cell (ii); **(c)** super resolution fluorescence microscopy of SFPQ (red) and FUS (green) co-staining following
461 transfection (i) and an untreated cell (ii); **(d)** super resolution fluorescence microscopy of NONO (red) and
462 LAMIN-B1 (green) co-staining following transfection (i-ii) and an untreated cell (iii). A single z-frame is shown in (i)
463 and a maximum intensity z-stack in (ii). For all SIM images scale bar = 5 µm.
464

465 *2´ O-methyl phosphorothioate AOs affect ribosomal RNA processing and maturation*

466 Since Cajal bodies and fibrillarin are important in ribosomal RNA processing and assembly,
467 we assessed rRNA levels in 2´ O-methyl phosphorothioate AO transfected cells and
468 untreated cells. qPCR and bioanalyser data show unprocessed rRNA was markedly increased
469 by 2´ O-methyl phosphorothioate AO transfection in fibroblasts (**Figure 4**). A Bioanalyser
470 RNA trace from 2´ O-methyl phosphorothioate control AO transfected fibroblasts (**Figure**
471 **4a**) showed low levels of 18S and 28S ribosomal subunits, as well as a number of
472 intermediate peaks compared to that on RNA from untreated fibroblasts (**Figure 4b**),
473 consistent with incomplete rRNA processing. Poor RNA quality was ruled out, given a
474 similar pattern was observed in all experimental repeats (n=6). This observation was
475 supported by qPCR analysis of rRNA levels showing a 2 to 3.5-fold increase in the level of
476 the unprocessed 45S rRNA in 2´ O-methyl phosphorothioate transfected compared to
477 untreated fibroblasts (**Figure 4c**). Unprocessed rRNA accumulated over time, following the
478 formation of nuclear inclusions (**Figure 4d**).

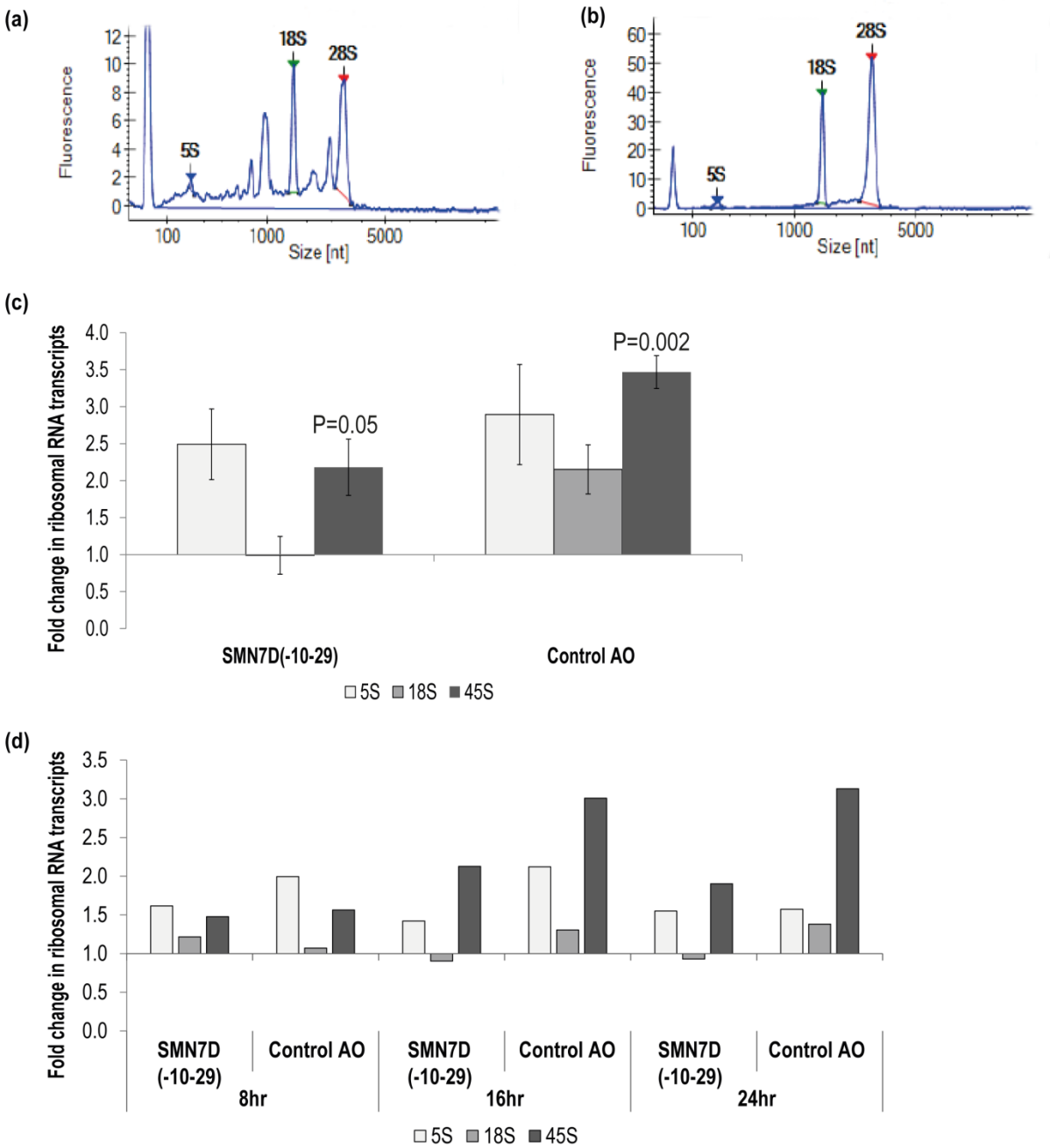

Figure 4 Analysis of ribosomal RNA processing, showing bioanalyser trace of rRNA from **(a)** 2´O-methyl phosphorothioate control AO transfected cells, and **(b)** untreated cells; **(c)** qPCR analysis of 5S, 18S and 45S rRNA levels following 2´O-methyl phosphorothioate transfection (24 hours). rRNA levels were normalised against *TBP* and compared to those in untreated cells where untreated = 1 (n=3). Error bars represent the standard error of the mean, and P-values were calculated using a paired student T-test; and **(d)** qPCR analysis of rRNA levels over 8, 16 and 24 hours; analysis as in **(c)** (n=1).

2´ O-methyl phosphorothioate AO transfection promotes apoptosis

Following phosphorothioate AO transfection of U2OS cells at 100 nM, live cell imaging was undertaken to evaluate caspase activation (**Figure 5a**). Nuclear inclusions were observed

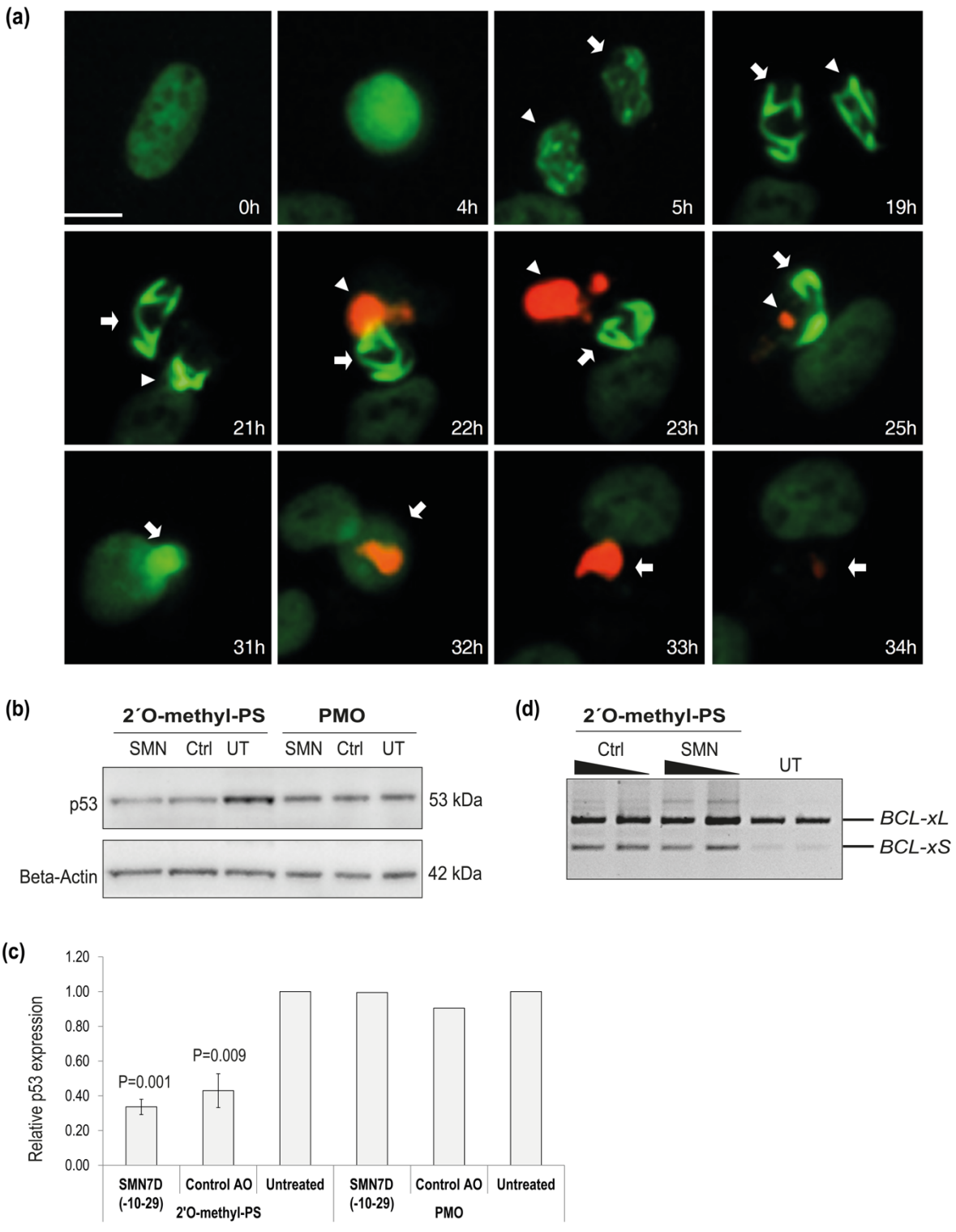

Figure 5 Analysis of cellular toxicity, showing **(a)** live cell imaging over time of U2OS cells with endogenous SFPQ-GFP (green) transfected with the 2´O-methyl phosphorothioate control AO and stained for caspase 3/7 activation (red). Two sister cells are annotated with arrows, and scale bar = 10 µm; **(b)** western blot of P53 and β-actin levels following 2´O-methyl phosphorothioate AO (n=3) and PMO transfection (n=1); **(c)** densitometry analysis of **(b)** where P53 levels are normalized to β-actin and compared to those in untreated cells where untreated = 1. Error bars represent the standard error of the mean and P-values were calculated using a paired

student T-test; and **(d)** RT-PCR analysis of *BCL2* transcripts following 2´O-methyl phosphorothioate AO transfection, as indicated at 100 and 50 nM (24 hours).

after 5 hours in two sister cells. Nuclear inclusions became larger and more compact overtime, followed by caspase activation after 22 hours. No caspase activation was observed in the absence of intranuclear inclusions, identifying nuclear inclusion as complicit in caspase activated apoptosis, leading to cell death. The tumour suppressor protein p53 was decreased, following transfection with 2´ O-methyl phosphorothioate AOs, relative to untreated control cells (**Figure 5b and c**), suggesting that the cell death observed was p53 independent, contrary to the findings by Shen *et al.,* 2018 (Shen *et al.* 2018) when using a 2′ fluoro-modified AO on a phosphorothioate backbone in the mouse. In comparison to phosphorothioate AO transfection, p53 levels remained unchanged following PMO transfection (**Figure 5b and c**).

The mitochondrial membrane and apoptosis regulating, *BCL2*-like gene encodes two alternatively spliced, functional protein isoforms, a longer anti-apoptotic isoform BCL-xL, and a shorter pro-apoptotic isoform BCL-xS. Increased abundance of the BCL-xS isoform induces cytochrome C release from the mitochondria, initiating caspase activated apoptosis. RT-PCR across the *BCL* transcripts (**Figure 5d**) shows 2´ O-methyl phosphorothioate AO transfection induces non-specific alternative splicing, increasing the levels of the pro-apoptotic *BCL-xS* transcript, potentially initiating the caspase activation shown in **Figure 5a**.

Transcriptome analysis of 2´ O-methyl phosphorothioate transfected cells reveals global cellular disruptions

We next evaluated the effect of 2´ O-methyl phosphorothioate transfection and nuclear inclusion formation on the transcriptome by RNA-seq. We prepared RNA from fibroblasts transfected with the two 2´ O-methyl phosphorothioate AOs used throughout this study as well as two control samples (untreated cells and cells transfected with a DNA phosphodiester AO (DNA control) version of the same sequence as the control AO, 100 nM for 24 hours) for RNAseq analysis (n=3). The RNAseq data is available at https://www.ncbi.nlm.nih.gov/geo/query/acc.cgi?acc=GSE121713 (accession number: GSE121713). An RNAseq heatmap comparing the expression of transcripts in 2´ O-methyl phosphorothioate AO transfected fibroblasts to that in cells transfected with the DNA phosphodiester oligonucleotide and untreated cells showed stark differences in expression

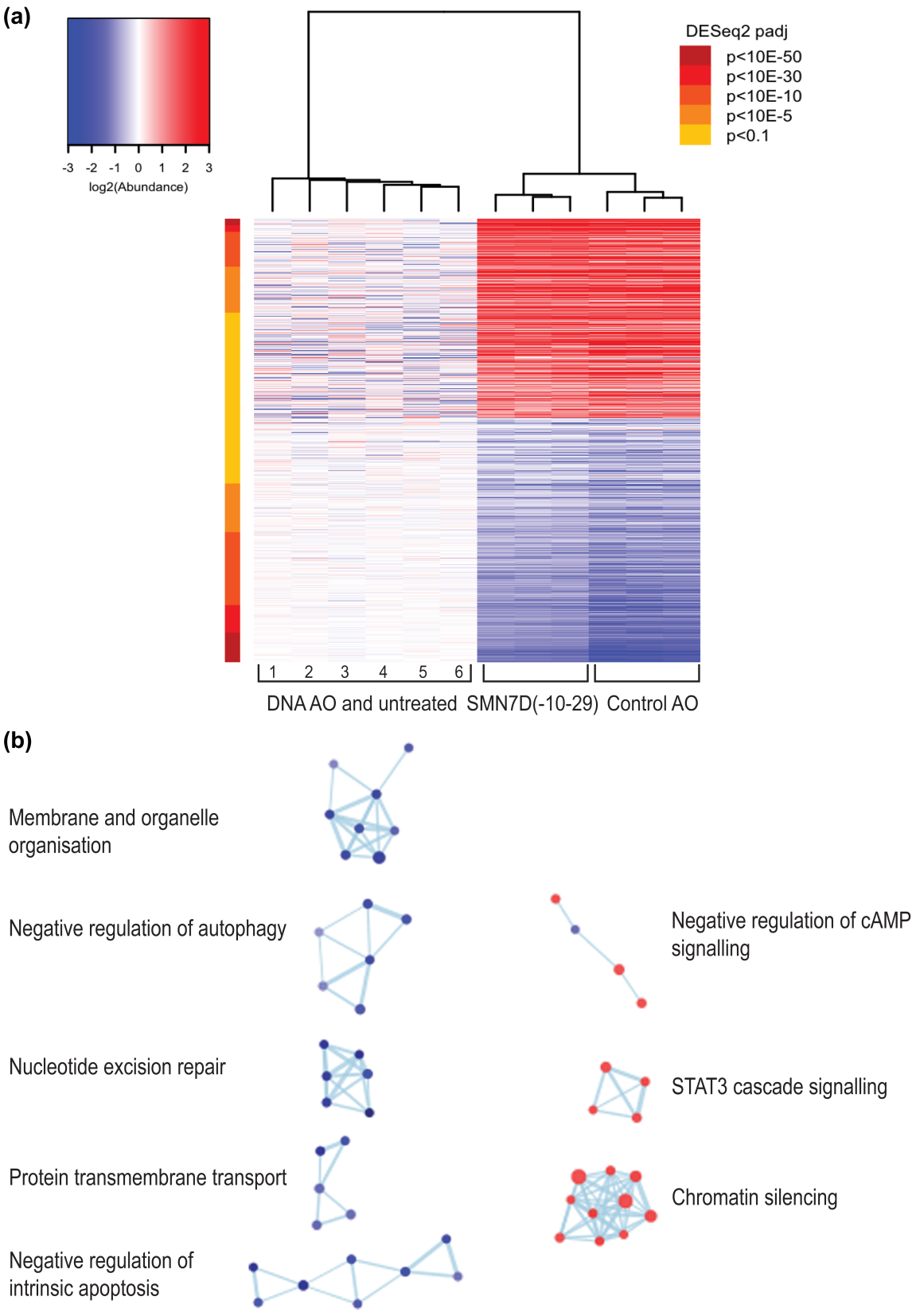

Figure 6 RNA sequencing analysis of fibroblasts showing **(a)** heatmap of all differentially expressed transcripts in control (1, 4, 5-untreated and 2, 3, 6, DNA AO) and 2´ O-methyl phosphorothioate AO *SMN7D(-10-20)* and control AO) transfected (100 nM, 24 hours) cells, whereby red represents overexpressed transcripts, and blue

represents under-expressed transcripts; and **(b)** gene ontology (GO) network of significantly affected cellular pathways in samples from transfected, compared to untreated and DNA AO transfected cells. GO terms are represented as dots being either overexpressed (red) or under-expressed (blue), and groups with greater than 50% of genes in common are linked.

between the groups (**Figure 6a**). Transcripts that are overexpressed in 2´ O-methyl phosphorothioate AO transfected cells compared to controls are indicated in red, while those that are underexpressed are indicated in blue.

Gene ontology (GO) analyses showed significant disruptions in transcripts involved in a number of major cellular pathways. The GO network (**Figure 6b**) revealed cellular processes and pathways that are significantly over-expressed include signaling pathways, chromatin silencing, and metabolic pathways, while those that are significantly under-expressed include negative regulation of apoptosis and autophagy, membrane and organelle organisation, protein transmembrane transport and nucleotide excision repair. Gene ontology pathways included in each cellular process are listed in **Supplementary File 2.** Thus, overall these data show dramatic and widespread changes to gene expression in human fibroblasts as a result of the uptake of the 2´ O-methyl phosphorothioate AOs.

Discussion

AOs have therapeutic potential as modulators of gene expression in many different diseases, and can do so through several different mechanisms. Antisense drugs that are in current clinical use alter exon selection during pre-mRNA processing, or induce RNaseH degradation of the target mRNA, the mechanism of action determined by the nature of the AO chemistry (for review see (Tri Le *et al.* 2016)). However, emerging reports of off-target effects conferred by synthetic oligonucleotides, identified *in vitro* (Shen *et al.* 2014, Shen *et al.* 2015) and *in vivo* (Shen *et al.* 2014, Shen *et al.* 2018), demand careful examination of the molecular effects of these compounds. Here we report that transfection of cultured human dermal fibroblasts, U2OS osteosarcoma cells, SH-SY5Y neuroblastoma cells and primary myogenic cells with 2´ O-methyl phosphorothioate oligonucleotides causes the formation of large structured nuclear inclusions, decorated with proteins that are normally components of nuclear organelles, in particular, paraspeckles. We show evidence that 2´ O-methyl phosphorothioate AO transfection alters the distribution of proteins normally associated with subnuclear bodies, impacts on global transcript expression and ribosomal RNA processing,

570 among other critical cellular processes, and induces cell stress, followed by apoptosis.

571

572 Interaction of phosphorothioate oligonucleotides with nuclear proteins, including certain
573 paraspeckle proteins, and the formation of paraspeckle-like structures, independent of
574 *NEAT1,* has been reported (Shen *et al.* 2014, Shen *et al.* 2015, Shen *et al.* 2018). While Shen
575 *et al.* (Shen *et al.* 2014) focused on the effect of phosphorothioate AOs on NONO and
576 reported altered paraspeckle structure, this was in the context of AO-mediated modulation of
577 gene expression, not the broader cell biology. Other off-target effects and non-specific
578 binding of proteins, initiated by the negatively charged phosphorothioate backbone have
579 been reported elsewhere (Dias and Stein 2002, Winkler *et al.* 2010, Liang *et al.* 2015).
580 Hence, our experience and extensive research usage of AOs prompted further investigation of
581 the global consequences of 2´ O-methyl phosphorothioate AO transfection on cell biology,
582 showing many significant changes, as described above. In contrast, the transfection of
583 (charge-neutral) PMOs in the current study did not disrupt subnuclear structures, or result in
584 any alteration in the distribution or staining intensity of the nuclear proteins studied. This
585 result was reproducible using multiple delivery techniques, including high dose, uncomplexed
586 PMO transfection, transfection of PMO annealed to a DNA leash and complexed with
587 liposome reagent, as well as nucleofection. In comparison, all 2´ O-methyl phosphorothioate
588 AO sequences tested induced novel, structured intranuclear inclusions, revealed by
589 transmission electron microscopy to have amyloid aggregate-like appearance.

590

591 The nuclear inclusions observed in phosphorothioate transfected cells are associated with
592 altered nuclear architecture, disturbed gene expression and ultimately, apoptosis. While
593 formation of such large, and apparently irreversible structures would be expected to impact on
594 nuclear biology, the likely consequences of aberrant sequestration of paraspeckle and other
595 nuclear proteins on RNA processing and post transcriptional regulation are of prime concern.
596 Paraspeckles are dynamic, RNA-protein nuclear organelles that occur in the interchromatin
597 space in mammalian cells and are now known to contain over 40 different proteins associated
598 with one architectural long non-coding RNA, *NEAT1_2* (for review see (Fox *et al.* 2018)).
599 Observed in most cultured cells-other than various stem cells, and cells experiencing stress,
600 paraspeckles regulate gene expression through sequestration of proteins and RNAs (Fox *et al.*
601 2018), but are also implicated in microRNA biogenesis (Jiang *et al.* 2017). Paraspeckle
602 proteins can undergo rapid, but normally reversible aggregation from monomers to form

603 amyloid-like structures, seeded by *NEAT1_2*, and likely mediated through prion-like domains
604 that are enriched in uncharged polar amino acids (Lancaster *et al.* 2014). The mechanism by
605 which phosphorothioate oligonucleotides induce some paraspeckle proteins to form aberrant
606 aggregates is unknown, however, we do know that sub cellular localization and
607 phosphorothioate AO behaviour in transfected cells is influenced by protein interactions and
608 the 2´ sugar AO modifications (Bailey *et al.* 2017, Crooke *et al.* 2017), and that synthetic
609 double stranded RNA is also able to seed *de novo* paraspeckle formation (Shelkovnikova *et*
610 *al.* 2018). How other nuclear proteins become incorporated into the phosphorothioate AO
611 induced nuclear inclusions, and why TDP43, a major component of paraspeckles does not
612 appear in these inclusions in our study, remains elusive.
613
614 Immunofluorescent staining of 2´ O-methyl phosphorothioate transfected fibroblasts revealed
615 the paraspeckle components NONO, PSPC1, SFPQ and FUS co-localised with large nuclear
616 structures in excess of 2000 nm in length, with FUS decorating the structures in an ordered
617 manner. All four of these proteins include prion-like domains (for review see (Fox *et al.*
618 2018)) and we speculate that the known propensity of phosphorothioate backbone compounds
619 to interact with and bind proteins then alters the liquid-liquid phase properties of the
620 paraspeckle proteins, shifting them towards insoluble, amyloid-like aggregations. However,
621 not all paraspeckle components with prion-like domains investigated were found to colocalise
622 with the inclusions, and in addition, the localisation and distribution of some proteins
623 associated with other subnuclear bodies was altered in cells with nuclear inclusions.
624
625 Coilin, an integral component of Cajal bodies, nucleolin, one of the most abundant proteins in
626 the nucleolus but also found in the cytoplasm and on the cell membrane, fibrillarin, located in
627 the dense fibrillar component of the nucleolus and SC35 (SRSF2), an essential splicing factor
628 found in nuclear speckles all showed altered distribution in cells that have phosphorothioate
629 AO -induced nuclear inclusions, but did not co-localize with these inclusions. Cajal bodies
630 assemble spliceosomal and nucleolar ribonucleoproteins required for pre-mRNA and pre-
631 rRNA processing, and are recently proposed to contribute to genome organization, with global
632 effects on gene expression and RNA splicing (Wang *et al.* 2016). The nucleolus is the most
633 prominent nuclear structure, and is where synthesis and processing of ribosomal transcripts to
634 yield the mature rRNAs *5.8S, 18S* and *28S* from the *45S* pre- rRNA takes place. We show that
635 ribosomal RNA processing is greatly impaired by 2´ O-methyl phosphorothioate AO

636 transfection, and speculate that this is a likely manifestation of improper localization of major
637 protein components of the nucleolus and Cajal bodies and consequent disruption to their
638 functions. In addition, the aberrant inclusions that we speculate occupy interchromosomal
639 spaces may well impose physical constraints upon nuclear organisation, and prevent proper
640 localisation of Cajal bodies and the nucleoli close to their normal chromosomal sites. Tissues
641 with high demand for transcript splicing and ribosome biogenesis, and neurons in particular,
642 have prominent Cajal bodies, juxtaposed to nucleoli (for review see (Lafarga *et al.* 2017)),
643 and disruption or loss of Cajal bodies is associated with severe neuronal dysfunction (Tapia *et*
644 *al.* 2017). Indeed, disruption or depletion of Cajal bodies was seen as the earliest nuclear sign
645 of motor neuron degeneration in a spinal muscular atrophy mouse model and induced a
646 progressive nucleolar dysfunction in ribosome biogenesis (Tapia *et al.* 2017).
647
648 Paraspeckle biology has gained increasing interest due to the association of paraspeckle
649 proteins with neurodegenerative disease, in particular amyotrophic lateral sclerosis (ALS),
650 and the observation that *NEAT1_2* is up-regulated in early-stage motor neurons from the
651 spinal cords of ALS patients (Shelkovnikova *et al.* 2014, Yamazaki and Hirose 2015).
652 Paraspeckle formation, not observed in healthy spinal motor neurons, is enhanced in spinal
653 cords of patients with early stage sporadic and familial ALS, and mutations in many
654 paraspeckle proteins (eg. TDP-43, FUS, NONO, SFPQ) are associated with ALS (Nishimoto
655 *et al.* 2013, Shelkovnikova *et al.* 2018). Whether paraspeckles are protective or causative in
656 ALS molecular pathology is not known at this time (Yamazaki and Hirose 2015), nor is the
657 role of paraspeckles in disease well understood. Nevertheless, phosphorothioate AO-
658 mediated dysregulation of paraspeckle formation and altered nucleoli and Cajal body biology
659 shown in our study, together with the building body of evidence that nuclear organelle
660 dysfunction (Lafarga *et al.* 2017, Tapia *et al.* 2017) has implications for central nervous
661 system, and probably all, clinical applications of these compounds.
662
663 Not surprisingly, considering the altered nuclear architecture and distribution of proteins
664 implicated in RNA biology, transcriptome sequencing showed significant global effects on the
665 expression of transcripts and revealed disturbances to many critical cellular processes in
666 phosphorothioate AO transfected cells. Of particular concern, pathways involved in apoptosis,
667 chromatin silencing, cellular metabolism and a number of signalling pathways, autophagy and
668 nucleotide excision repair were disturbed. While we acknowledge that these *in vitro* studies in

669 replicating cells may not fully reflect potential off-target treatment effects in tissues *in vivo*,
670 Toonan et al., 2018 (Toonen *et al.* 2018) report significant upregulation of immune system-
671 associated genes in brains of mice treated by intracerebroventricular injection of 2′ O-methyl
672 phosphorothioate AO. The upregulation of immune system associated genes was detectable for
673 at least 2 months after the last AO administration. Here, the exaggerated sequestration of
674 nuclear proteins as a result of 2′ O-methyl phosphorothioate AO transfection dramatically
675 disturbs RNA processing, disrupts nuclear architecture, and induces apoptosis, and it seems
676 reasonable to consider that injection site reactions and adverse effects reported after clinical
677 evaluation of the 2′ O-methyl phosphorothioate *Drisapersen* for the treatment of Duchenne
678 muscular dystrophy (Mendell *et al.* 2017) and *Kynamro*® (*Mipomersen*) for the treatment of
679 familial hypercholesterolemia (Wong and Goldberg 2014) may be mediated at least in part, by
680 non-specific interactions of nuclear components with the AO backbone. It might also be
681 prudent to deliberate on the reported effects of antisense drugs, attributed to the AO action on
682 the target transcript, and consider whether some level of the apparent antisense effect on
683 splicing, in particular, could perhaps be a consequence of disturbance of RNA processing
684 pathways more broadly.
685
686 We speculate that, unlike endogenous paraspeckles and other dynamic nuclear bodies, the
687 formation of the aberrant nuclear inclusions seen *in vitro* here does not appear to be
688 reversible. While 2′ O-methyl phosphorothioate transfected cultures showed reduced cell
689 numbers, whether this was due to cell death or impaired replication, or both, is uncertain, and
690 whether the nuclear inclusions *per se* or reduced availability of RNA processing are primarily
691 responsible requires further investigation. However, any effects resulting in perturbation of
692 nuclear proteins may be compounded by the formation of the nuclear amyloid-like
693 aggregates and likely disturbance of protein homeostasis, termed 'proteostasis' (Yerbury *et*
694 *al.* 2016). Although other descriptions of exogenously induced nuclear amyloid-like
695 aggregates are limited, Arnhold *et al.,* 2015 (Arnhold *et al.* 2015) identified large amyloid-
696 like aggregates in SH-SY5Y cells, treated with mercury, a notorious neurotoxicant, in a study
697 that explains the mechanism of heavy metal neurotoxicity and identified amyloid protein
698 aggregation in the cell nucleus as causative. Mass spectrometry of the purified protein
699 aggregates identified a subset of spliceosomal components and the nuclear envelope protein
700 lamin B1 (Arnhold *et al.* 2015). In our study, we also detected changes in lamin B1, although
701 here we did not detect lamin B1 in the nuclear inclusions, we nevertheless observed that

702 nuclear membrane and lamin B1 organization was distorted in fibroblasts containing nuclear
703 inclusions. Interestingly, the multi-lobulated nuclei and lamin B1 staining are reminiscent of
704 cells from progeria patients carrying the lamin A 433G>A mutation (E145K) (Taimen *et al.*
705 2009).
706

707 In summary, we report phosphorothioate backbone-specific effects of modified
708 oligonucleotides on the distribution and localization of nuclear proteins, appearance of novel
709 nuclear structures composed in part of a subset of paraspeckle protein components, and
710 sequence-independent effects on nascent RNA processing. While the *in vivo,* longer term
711 repercussions of exogenous oligonucleotide-induced nuclear protein aggregates that include
712 many paraspeckle components and cause sub-nuclear disorganisation are yet to be
713 determined, our observations suggest that phosphorothioate backbone antisense compounds
714 destined for clinical application would benefit from further scrutiny.
715

716 **Acknowledgments**

717 The authors would like to acknowledge technical advice from Russell Johnsen. This work was
718 performed in part during LLF's and ILP's PhD candidatures. Laboratory studies and ILP were
719 supported by funding from the Parry Foundation through the Spinal Muscular Atrophy
720 Association of Australia and LLF received a Team Spencer and Muscular Dystrophy WA PhD
721 stipend. The authors received research support from the NHMRC Project Grants
722 APP1147496, APP1086311, APP1144791 and the MNDi foundation, Western Australia.
723

724 **Author Contributions**

725 Conceived and designed experiments: LLF, RL, SF, MTA, ILP and AF. Performed
726 experiments: LLF, RL, MTA, ILP, AH, and LG. Analysis of RNA-seq data: JC. Prepared and
727 edited manuscript: LLF, SF, RL, MTA, ILP, JC, AH, LG, SDW and AF.
728 Declaration of interests: SF and SDW act as consultants to Sarepta Therapeutics and are
729 named inventors of patents licensed through the University of Western Australia to Sarepta
730 Therapeutics. As such, they are entitled to milestone and royalty payments that may be
731 generated from licensing agreements and are involved in ongoing collaborative research
732 projects with Sarepta Therapeutics.
733
734
735

736 **References:**

737 AM Adams, PL Harding, PL Iversen, C Coleman, S Fletcher and SD Wilton (2007).
738 **Antisense oligonucleotide induced exon skipping and the dystrophin gene**
739 **transcript: Cocktails and chemistries**. *BMC Mol Biol* **8**: 57
740
741 F Arnhold, KH Guhrs and A von Mikecz (2015). **Amyloid domains in the cell nucleus**
742 **controlled by nucleoskeletal protein lamin b1 reveal a new pathway of mercury**
743 **neurotoxicity**. *PeerJ* **3**: e754.10.7717/peerj.754

JK Bailey, W Shen, XH Liang and ST Crooke (2017). **Nucleic acid binding proteins affect the subcellular distribution of phosphorothioate antisense oligonucleotides**. *Nucleic Acids Res* **45**(18): 10649-10671.10.1093/nar/gkx709

CF Bennett, BF Baker, N Pham, E Swayze and RS Geary (2017). **Pharmacology of antisense drugs**. *Annu Rev Pharmacol Toxicol* **57**: 81-105.10.1146/annurev-pharmtox-010716-104846

CS Bond and AH Fox (2009). **Paraspeckles: Nuclear bodies built on long noncoding rna**. *J Cell Biol* **186**(5): 637-644.10.1083/jcb.200906113

M Chakravarthy, S Chen, PR Dodd and RN Veedu (2017). **Nucleic acid-based theranostics for tackling alzheimer's disease**. *Theranostics* **7**(16): 3933-3947.10.7150/thno.21529

ST Crooke, S Wang, TA Vickers, W Shen and XH Liang (2017). **Cellular uptake and trafficking of antisense oligonucleotides**. *Nat Biotechnol* **35**(3): 230-237.10.1038/nbt.3779

N Dias and CA Stein (2002). **Potential roles of antisense oligonucleotides in cancer therapy. The example of bcl-2 antisense oligonucleotides**. *Eur J Pharm Biopharm* **54**(3): 263-269

S Fletcher, K Honeyman, AM Fall, PL Harding, RD Johnsen and SD Wilton (2006). **Dystrophin expression in the mdx mouse after localised and systemic administration of a morpholino antisense oligonucleotide**. *J Gene Med* **8**(2): 207-216

U Flierl, TL Nero, B Lim, JF Arthur, Y Yao, SM Jung, E Gitz, AY Pollitt, MT Zaldivia, M Jandrot-Perrus, A Schafer, B Nieswandt, RK Andrews, MW Parker, EE Gardiner and K Peter (2015). **Phosphorothioate backbone modifications of nucleotide-based drugs are potent platelet activators**. *J Exp Med* **212**(2): 129-137.10.1084/jem.20140391

AH Fox, S Nakagawa, T Hirose and CS Bond (2018). **Paraspeckles: Where long noncoding rna meets phase separation**. *Trends Biochem Sci* **43**(2): 124-135.10.1016/j.tibs.2017.12.001

BL Gebski, CJ Mann, S Fletcher and SD Wilton (2003). **Morpholino antisense oligonucleotide induced dystrophin exon 23 skipping in mdx mouse muscle**. *Hum Mol Genet* **12**(15): 1801-1811

L Jiang, C Shao, QJ Wu, G Chen, J Zhou, B Yang, H Li, LT Gou, Y Zhang, Y Wang, GW Yeo, Y Zhou and XD Fu (2017). **Neat1 scaffolds rna-binding proteins and the microprocessor to globally enhance pri-mirna processing**. *Nat Struct Mol Biol* **24**(10): 816-824.10.1038/nsmb.3455

M Kinali, V Arechavala-Gomeza, L Feng, S Cirak, D Hunt, C Adkin, M Guglieri, E Ashton, S Abbs, P Nihoyannopoulos, ME Garralda, M Rutherford, C McCulley, L Popplewell, IR Graham, G Dickson, MJ Wood, DJ Wells, SD Wilton, R Kole, V Straub, K Bushby, C Sewry, JE Morgan and F Muntoni (2009). **Local restoration of dystrophin expression with the morpholino oligomer avi-4658 in duchenne muscular dystrophy: A single-**

blind, placebo-controlled, dose-escalation, proof-of-concept study. *Lancet Neurol* **8**(10): 918-928.S1474-4422(09)70211-X [pii] 10.1016/S1474-4422(09)70211-X

M Lafarga, O Tapia, AM Romero and MT Berciano (2017). **Cajal bodies in neurons**. *RNA Biol* **14**(6): 712-725.10.1080/15476286.2016.1231360

AK Lancaster, A Nutter-Upham, S Lindquist and OD King (2014). **Plaac: A web and command-line application to identify proteins with prion-like amino acid composition**. *Bioinformatics* **30**(17): 2501-2502.10.1093/bioinformatics/btu310

R Li, AR Harvey, SI Hodgetts and AH Fox (2017). **Functional dissection of neat1 using genome editing reveals substantial localization of the neat1_1 isoform outside paraspeckles**. *RNA* **23**(6): 872-881.10.1261/rna.059477.116

S Li, FJ Shu, Z Li, L Jaafar, S Zhao and WS Dynan (2017). **Cell-type specific role of the rna-binding protein, nono, in the DNA double-strand break response in the mouse testes**. *DNA Repair (Amst)* **51**: 70-78.10.1016/j.dnarep.2017.02.002

XH Liang, H Sun, W Shen and ST Crooke (2015). **Identification and characterization of intracellular proteins that bind oligonucleotides with phosphorothioate linkages**. *Nucleic Acids Res* **43**(5): 2927-2945.10.1093/nar/gkv143

F Lipi, S Chen, M Chakravarthy, S Rakesh and RN Veedu (2016). **In vitro evolution of chemically-modified nucleic acid aptamers: Pros and cons, and comprehensive selection strategies**. *RNA Biol* **13**(12): 1232-1245.10.1080/15476286.2016.1236173

JR Mendell, N Goemans, LP Lowes, LN Alfano, K Berry, J Shao, EM Kaye, E Mercuri, G Eteplirsen Study and DMDIN Telethon Foundation (2016). **Longitudinal effect of eteplirsen versus historical control on ambulation in duchenne muscular dystrophy**. *Ann Neurol* **79**(2): 257-271.10.1002/ana.24555

JR Mendell, LR Rodino-Klapac, Z Sahenk, K Roush, L Bird, LP Lowes, L Alfano, AM Gomez, S Lewis, J Kota, V Malik, K Shontz, CM Walker, KM Flanigan, M Corridore, JR Kean, HD Allen, C Shilling, KR Melia, P Sazani, JB Saoud, EM Kaye and G Eteplirsen Study (2013). **Eteplirsen for the treatment of duchenne muscular dystrophy**. *Ann Neurol* **74**(5): 637-647.10.1002/ana.23982

JR Mendell, Z Sahenk and L Rodino-Klapac (2017). **Clinical trials of exon skipping in duchenne muscular dystrophy**. *Expert Opinion on Orphan Drugs* **5**(9): 683-690.DOI: 10.1080/21678707.2017.1366310

C Mitrpant, P Porensky, H Zhou, L Price, F Muntoni, S Fletcher, SD Wilton and AH Burghes (2013). **Improved antisense oligonucleotide design to suppress aberrant smn2 gene transcript processing: Towards a treatment for spinal muscular atrophy**. *PLoS One* **8**(4): e62114.10.1371/journal.pone.0062114

T Naganuma, S Nakagawa, A Tanigawa, YF Sasaki, N Goshima and T Hirose (2012). **Alternative 3'-end processing of long noncoding rna initiates construction of nuclear paraspeckles**. *EMBO J* **31**(20): 4020-4034.10.1038/emboj.2012.251

Y Nishimoto, S Nakagawa, T Hirose, HJ Okano, M Takao, S Shibata, S Suyama, K Kuwako, T Imai, S Murayama, N Suzuki and H Okano (2013). **The long non-coding rna nuclear-enriched abundant transcript 1_2 induces paraspeckle formation in the motor neuron during the early phase of amyotrophic lateral sclerosis**. *Mol Brain* **6**: 31.10.1186/1756-6606-6-31

DM Paton (2017). **Nusinersen: Antisense oligonucleotide to increase smn protein production in spinal muscular atrophy**. *Drugs Today (Barc)* **53**(6): 327-337.10.1358/dot.2017.53.6.2652413

TA Shelkovnikova, MS Kukharsky, H An, P Dimasi, S Alexeeva, O Shabir, PR Heath and VL Buchman (2018). **Protective paraspeckle hyper-assembly downstream of tdp-43 loss of function in amyotrophic lateral sclerosis**. *Mol Neurodegener* **13**(1): 30.10.1186/s13024-018-0263-7

TA Shelkovnikova, HK Robinson, C Troakes, N Ninkina and VL Buchman (2014). **Compromised paraspeckle formation as a pathogenic factor in fusopathies**. *Human Molecular Genetics* **23**(9): 2298-2312.10.1093/hmg/ddt622

L Shen, A Frazer-Abel, PR Reynolds, PC Giclas, A Chappell, MK Pangburn, H Younis and SP Henry (2014). **Mechanistic understanding for the greater sensitivity of monkeys to antisense oligonucleotide-mediated complement activation compared with humans**. *J Pharmacol Exp Ther* **351**(3): 709-717.10.1124/jpet.114.219378

W Shen, CL De Hoyos, H Sun, TA Vickers, XH Liang and ST Crooke (2018). **Acute hepatotoxicity of 2' fluoro-modified 5-10-5 gapmer phosphorothioate oligonucleotides in mice correlates with intracellular protein binding and the loss of dbhs proteins**. *Nucleic Acids Res* **46**(5): 2204-2217.10.1093/nar/gky060

W Shen, XH Liang and ST Crooke (2014). **Phosphorothioate oligonucleotides can displace neat1 rna and form nuclear paraspeckle-like structures**. *Nucleic Acids Res* **42**(13): 8648-8662.10.1093/nar/gku579

W Shen, XH Liang, H Sun and ST Crooke (2015). **2'-fluoro-modified phosphorothioate oligonucleotide can cause rapid degradation of p54nrb and psf**. *Nucleic Acids Res* **43**(9): 4569-4578.10.1093/nar/gkv298

NK Singh, NN Singh, EJ Androphy and RN Singh (2006). **Splicing of a critical exon of human survival motor neuron is regulated by a unique silencer element located in the last intron**. *Mol Cell Biol* **26**(4): 1333-1346.10.1128/MCB.26.4.1333-1346.2006

CA Stein and D Castanotto (2017). **Fda-approved oligonucleotide therapies in 2017**. *Mol Ther* **25**(5): 1069-1075.10.1016/j.ymthe.2017.03.023

P Taimen, K Pfleghaar, T Shimi, D Moller, K Ben-Harush, MR Erdos, SA Adam, H Herrmann, O Medalia, FS Collins, AE Goldman and RD Goldman (2009). **A progeria mutation reveals functions for lamin a in nuclear assembly, architecture, and chromosome organization**. *Proc Natl Acad Sci U S A* **106**(49): 20788-20793.10.1073/pnas.0911895106

O Tapia, JO Narcis, J Riancho, O Tarabal, L Piedrafita, J Caldero, MT Berciano and M Lafarga (2017). **Cellular bases of the rna metabolism dysfunction in motor neurons of a murine model of spinal muscular atrophy: Role of cajal bodies and the nucleolus**. *Neurobiol Dis* **108**: 83-99.10.1016/j.nbd.2017.08.004

LJA Toonen, J Casaca-Carreira, M Pellise-Tintore, H Mei, Y Temel, A Jahanshahi and WMC van Roon-Mom (2018). **Intracerebroventricular administration of a 2'-o-methyl phosphorothioate antisense oligonucleotide results in activation of the innate immune system in mouse brain**. *Nucleic Acid Ther* **28**(2): 63-73.10.1089/nat.2017.0705

B Tri Le, RN Veedu, S Fletcher and SD Wilton (2016). **Antisense oligonucleotide development for the treatment of muscular dystrophies**. *Expert Opinion on Orphan Drugs* **4**(2): 139-152.10.1517/21678707.2016.1122517

RN Veedu (2015). **Medicinal chemistry of aptamers**. *Curr Top Med Chem* **15**(12): 1065

Q Wang, IA Sawyer, MH Sung, D Sturgill, SP Shevtsov, G Pegoraro, O Hakim, S Baek, GL Hager and M Dundr (2016). **Cajal bodies are linked to genome conformation**. *Nat Commun* **7**: 10966.10.1038/ncomms10966

SD Wilton, RN Veedu and S Fletcher (2015). **The emperor's new dystrophin: Finding sense in the noise**. *Trends Mol Med* **21**(7): 417-426.10.1016/j.molmed.2015.04.006

J Winkler, M Stessl, J Amartey and CR Noe (2010). **Off-target effects related to the phosphorothioate modification of nucleic acids**. *ChemMedChem* **5**(8): 1344-1352.10.1002/cmdc.201000156

E Wong and T Goldberg (2014). **Mipomersen (kynamro): A novel antisense oligonucleotide inhibitor for the management of homozygous familial hypercholesterolemia**. *P T* **39**(2): 119-122

T Yamazaki and T Hirose (2015). **The building process of the functional paraspeckle with long non-coding rnas**. *Front Biosci (Elite Ed)* **7**: 1-41

JJ Yerbury, L Ooi, A Dillin, DN Saunders, DM Hatters, PM Beart, NR Cashman, MR Wilson and H Ecroyd (2016). **Walking the tightrope: Proteostasis and neurodegenerative disease**. *Journal of Neurochemistry* **137**(4): 489-505.10.1111/jnc.13575

934